

Bandgap and optical absorption edge of GaAs_{1-x}Bi_x alloys with 0

M. Masnadi-Shirazi, R. B. Lewis, V. Bahrami-Yekta, T. Tiedje, M. Chicoine, and P. Servati

Citation: *Journal of Applied Physics* **116**, 223506 (2014); doi: 10.1063/1.4904081

View online: <http://dx.doi.org/10.1063/1.4904081>

View Table of Contents: <http://scitation.aip.org/content/aip/journal/jap/116/22?ver=pdfcov>

Published by the [AIP Publishing](#)

Articles you may be interested in

Accurate determination of optical bandgap and lattice parameters of Zn_{1-x}Mg_xO epitaxial films ($0 \leq x \leq 0.3$) grown by plasma-assisted molecular beam epitaxy on a-plane sapphire

J. Appl. Phys. **113**, 233512 (2013); 10.1063/1.4811693

Ge_{1-y}Sn_y/Si (100) composite substrates for growth of In_xGa_{1-x}As and GaAs_{1-x}Sb_x alloys

J. Appl. Phys. **101**, 013518 (2007); 10.1063/1.2407274

Structural and optical properties of GaN_{1-x}As_x grown by metalorganic chemical vapor deposition

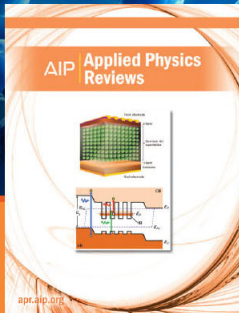
Appl. Phys. Lett. **85**, 4361 (2004); 10.1063/1.1819513

Effects of ordering and alloy phase separation on the optical emission characteristics of In_{1-x}Ga_xAs_yP_{1-y} layers grown on GaAs substrates

J. Appl. Phys. **89**, 4898 (2001); 10.1063/1.1360218

Structural and optical properties of pseudomorphic In_xGa_{1-x}N alloys

Appl. Phys. Lett. **73**, 1757 (1998); 10.1063/1.122272



NEW Special Topic Sections

NOW ONLINE
Lithium Niobate Properties and Applications:
Reviews of Emerging Trends

AIP | Applied Physics Reviews

Bandgap and optical absorption edge of GaAs_{1-x}Bi_x alloys with 0 < x < 17.8%

M. Masnadi-Shirazi,^{1,2,a)} R. B. Lewis,^{2,3,b)} V. Bahrami-Yekta,² T. Tiedje,² M. Chicoine,⁴ and P. Servati¹

¹Department of Electrical and Computer Engineering, University of British Columbia, Vancouver, British Columbia V6T 1Z4, Canada

²Department of Electrical and Computer Engineering, University of Victoria, Victoria, British Columbia V8W 2Y2, Canada

³Department of Physics and Astronomy, University of British Columbia, Vancouver, British Columbia V6T 1Z1, Canada

⁴Département de Physique, Université de Montréal, Montréal, Québec H3C 3J7, Canada

(Received 15 September 2014; accepted 2 December 2014; published online 11 December 2014)

The compositional dependence of the fundamental bandgap of pseudomorphic GaAs_{1-x}Bi_x layers on GaAs substrates is studied at room temperature by optical transmission and photoluminescence spectroscopies. All GaAs_{1-x}Bi_x films (0 ≤ x ≤ 17.8%) show direct optical bandgaps, which decrease with increasing Bi content, closely following density functional theory predictions. The smallest measured bandgap is 0.52 eV (~2.4 μm) at 17.8% Bi. Extrapolating a fit to the data, the GaAs_{1-x}Bi_x bandgap is predicted to reach 0 eV at 35% Bi. Below the GaAs_{1-x}Bi_x bandgap, exponential absorption band tails are observed with Urbach energies 3–6 times larger than that of bulk GaAs. The Urbach parameter increases with Bi content up to 5.5% Bi, and remains constant at higher concentrations. The lattice constant and Bi content of GaAs_{1-x}Bi_x layers (0 < x ≤ 19.4%) are studied using high resolution x-ray diffraction and Rutherford backscattering spectroscopy. The relaxed lattice constant of hypothetical zincblende GaBi is estimated to be 6.33 ± 0.05 Å, from extrapolation of the Rutherford backscattering spectrometry and x-ray diffraction data. © 2014 AIP Publishing LLC. [<http://dx.doi.org/10.1063/1.4904081>]

INTRODUCTION

Bismuth-containing III–V semiconducting alloys have attracted attention due to the large bandgap (E_g) reduction observed with incorporation of small amounts of Bi, potentially allowing the wavelength range for GaAs-based devices, which absorb and emit infrared light to be extended. In GaAs_{1-x}Bi_x, the bandgap reduction is ~83 meV/% at low Bi concentrations (x ≤ 5%),^{1,2} which is much larger than the effect of In and Sb (17 meV/% In, 19 meV/% Sb)^{3,4} and only lower than the effect of N alloying (125 meV/% N in 0 ≤ x ≤ 2% range).⁵ Incorporation of Bi in GaAs_{1-x}Bi_x increases the spin–orbit splitting, and for x > 10%, the energy splitting of the split-off hole band exceeds the bandgap.⁶ This feature in the band structure will suppress an important Auger recombination channel and improve the performance of semiconductor lasers with Bi-containing active layers. Photoluminescence with emission wavelength up to 1.44 μm has previously been observed in GaAs_{1-x}Bi_x alloys with x ≤ 10.6% Bi.¹ As a result of growth challenges, until recently, the incorporation of high amounts of Bi (~x > 13%) into GaAs_{1-x}Bi_x films had not been achieved. The authors have recently demonstrated that highly crystalline GaAs_{1-x}Bi_x alloys with Bi contents up to 22% can be grown on GaAs substrates at temperatures as low as 200 °C by molecular beam epitaxy (MBE).⁷ This result raises the

question: what is the optical bandgap of these new non-dilute alloys? Material with the expected low bandgap (~ E_g ≤ 0.8 eV) is desirable for optoelectronic applications in the near and mid-infrared spectral range. It is noteworthy to mention that recently a number of III–V bismide semiconductor alloys, including GaSb_{1-x}Bi_x,⁸ InAs_{1-x}Bi_x,⁹ and In_xGa_{1-x}As_{1-y}Bi_y,^{10,11} have been grown by MBE on GaSb, InAs and InP substrates, respectively, demonstrating bandgap energies of less than 0.8 eV.

To address the above question, we used room temperature optical transmission spectroscopy to measure the fundamental optical bandgap and absorption coefficient of thin, pseudomorphic GaAs_{1-x}Bi_x films (0 ≤ x ≤ 17.8%) on GaAs substrates. These measurements reveal the composition dependence of E_g in this previously unexplored composition range. Moreover, the structural quality, lattice constant and Bi composition of the GaAs_{1-x}Bi_x layers (0 < x ≤ 19.4%) are studied using high resolution x-ray diffraction (HRXRD) and Rutherford backscattering spectroscopy (RBS). RBS is an excellent method for determination of Bi content, due to the large mass of Bi relative to Ga and As.

EXPERIMENT

A set of nominally undoped GaAs_{1-x}Bi_x layers (0 < x ≤ 19.4%) were grown on 350 μm thick single-side polished semi-insulating GaAs (001) substrates in a VG-V80H MBE reactor. During operation, the MBE shroud was cooled to ~-80 °C with a polysiloxane heat transfer fluid, instead of conventional liquid nitrogen cooling.^{12,13} Each sample consists of a 300–500 nm GaAs buffer layer,

^{a)}Author to whom correspondence should be addressed. Electronic mail: mostafam@ece.ubc.ca

^{b)}Present address: Paul-Drude-Institut für Festkörperelektronik, Hausvogteiplatz 5–7, 10117 Berlin, Germany

followed by a $\text{GaAs}_{1-x}\text{Bi}_x$ layer grown at low temperatures ($220^\circ\text{C} < T_{\text{sub}} < 360^\circ\text{C}$). The growth procedure is described in detail elsewhere.⁷ Layers with $x > 10\%$ Bi were grown at low temperatures ($220^\circ\text{C} < T_{\text{sub}} < 250^\circ\text{C}$) at or below the stoichiometric $\text{As}_2\text{:Ga}$ flux ratio (i.e., Ga-rich conditions).⁷ The thickness of the layers was gradually decreased from 450 to 20 nm with increasing Bi content, to avoid strain relaxation and also to minimize surface roughening due to build-up of Ga-Bi droplets on the surface. Layers covered with metallic droplets were subsequently etched in an $\text{HCl:H}_2\text{O}$ solution (1:4 ratio) for 2 min to remove the droplets. This greatly reduced the light scattered from the sample surface during the measurements. Removing the droplets by wet etching caused a $\sim 2\times$ increase in the photoluminescence (PL) emission in case of the 10.5% Bi sample that was heavily covered with surface droplets. Removal of the surface droplets was confirmed by scanning electron microscope (SEM). As an example, SEM images of the surface of a 13.5% Bi film before and after etching the droplets are shown in Fig. 1 for comparison. We note that etched layers with $x > 9\%$ Bi showed surface roughness in SEM due to non-uniform growth around the droplets.

Optical transmission measurements were performed at room temperature on the $\text{GaAs}_{1-x}\text{Bi}_x/\text{GaAs}$ heterostructures and on a GaAs reference substrate with the same thickness. In this experiment, white light from a halogen bulb was chopped at 200 Hz and focused on the entry slit of a Oriol Cornerstone 260 monochromator. The samples were illuminated at normal incidence with monochromatic light and the transmitted light was detected using un-cooled Ge (800–1750 nm) and PbS (1000–2900 nm) photodetectors, connected to a lock-in amplifier, and a combination of optical long-pass filters. In this experiment, the back surface of the substrate wafer was placed close to the detector to maximize the collection of transmitted specular and scattered light. The transmission spectra of only the $\text{GaAs}_{1-x}\text{Bi}_x$ layer was isolated by dividing the spectra of the $\text{GaAs}_{1-x}\text{Bi}_x/\text{GaAs}$ heterostructure by that of the GaAs reference sample ($T_{\text{GaAsBi}}/T_{\text{GaAs}}$). The $\text{GaAs}_{1-x}\text{Bi}_x$ sample and a reference substrate were measured right after each other to minimize any possible drift in optical power. The bandgap E_g and optical absorption coefficient are obtained from the resulting

spectra. Samples with up to 10.5% Bi content were also excited with a 532 nm 20 ns pulsed diode-pumped solid state laser at room temperature for photoluminescence (PL) measurements. The average power of the laser was 1.5 mW, at a repetition rate of 2 kHz and peak power density of 10^5W/cm^2 . The PL was dispersed using a SpectraPro-300i spectrograph and then detected by a liquid nitrogen-cooled InGaAs array detector. All the PL spectra were corrected for spectrometer throughput.

Unsuccessful attempts were made to measure the PL emission from high Bi content $\text{GaAs}_{1-x}\text{Bi}_x$ samples (i.e., $x > 11\%$) with the above-mentioned PbS photodetector. PL could not be detected, as the high Bi content samples are relatively thin ($d \leq 70 \text{ nm}$) and they were grown at low temperatures and not optimized for PL emission. In addition, the un-cooled PbS photodetector is not ideal for PL experiments as it has a relatively low detectivity at room temperature.

RBS measurements were performed using 2 MeV alpha particles. The detector was placed at a scattering angle of 170° , and the sample was tilted $\sim 7^\circ$ from the surface normal to minimize channeling effects. The compositions and layer thicknesses were obtained by simulating the RBS spectra using the SIMNRA software.¹⁴ High resolution x-ray diffraction (HRXRD) measurements were performed with a Bruker D8 Discover diffractometer. The (004) θ - 2θ scans and (224) reciprocal space maps (RSMs) were recorded to measure the in-plane and out-of-plane lattice constants, layer thicknesses, and degree of relaxation in the $\text{GaAs}_{1-x}\text{Bi}_x$ films. The (004) scans were dynamically simulated using LEPTOS software.

RESULTS AND DISCUSSION

Figure 2 shows (004) θ - 2θ HRXRD scans for several $\text{GaAs}_{1-x}\text{Bi}_x$ films on GaAs substrates used for optical transmission and PL experiments. In each rocking curve, the sharp peak corresponds to the GaAs buffer and substrate layers and the split off peak on the left corresponds to the $\text{GaAs}_{1-x}\text{Bi}_x$ layer. As expected, increasing the Bi content of the epilayer increases the lattice constant and shifts the split off peak to lower diffraction angles. With the exception of the 9.7% Bi sample (layer c), which is discussed below, θ - 2θ scans show pendellösung fringes, indicating good film uniformity and sharp interfaces. The composition and thickness

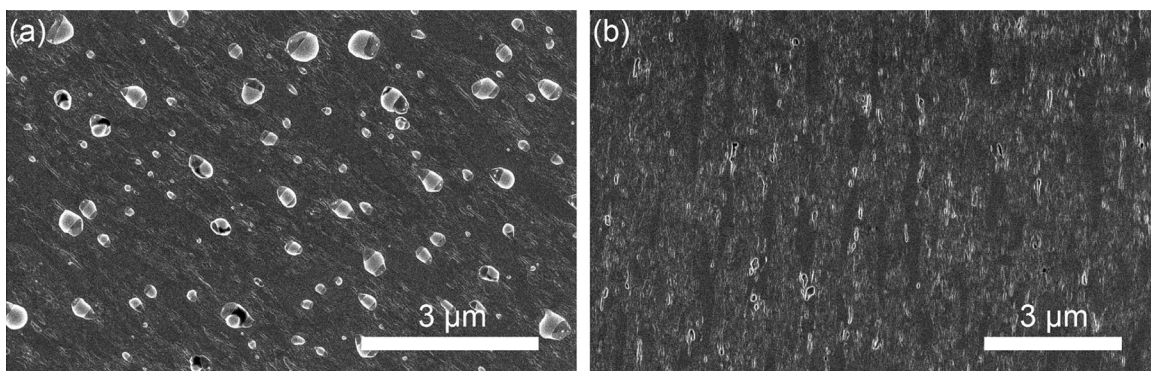


FIG. 1. SEM images of the surface of a 13.5% Bi film (a) before and (b) after etching the droplets with $\text{HCl:H}_2\text{O}$ solution. The dark side of the droplets in (a) is Bi, and the light side of the droplets is Ga. Energy-dispersive X-ray spectroscopy measurements on similar droplets confirm the composition of the droplets. The visible surface roughness of the etched sample is due to non-uniform growth around the droplets.

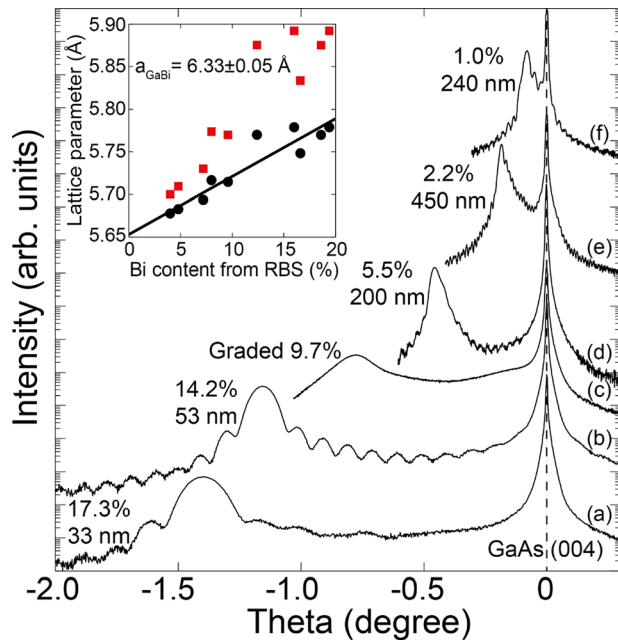


FIG. 2. (004) θ - 2θ HRXRD scans of GaAs_{1-x}Bi_x films on GaAs. Scans are offset vertically for clarity. The composition and thickness of the layers are determined from dynamical simulations. The sample with 9.7% Bi and no thickness fringes showed composition variation in the growth direction in RBS. The inset shows the measured strained out-of-plane lattice parameter (red squares) and corresponding relaxed lattice parameter (black circles) assuming a Poisson ratio of 0.31, as a function of the RBS Bi content. The GaBi lattice parameter is indicated from the extrapolation of the best fit (solid line).

of each film in this figure were determined by simulating the curves using LEPTOS (simulations not shown), assuming a pseudomorphic growth and employing the relationship between the lattice parameter and Bi content obtained from HRXRD and RBS measurements, as discussed below.

X-ray reciprocal space maps (RSM) of the (224) off-axis peaks on the samples with 2.2%, 5.5%, 9.7%, and 14.2% Bi in Fig. 2 and a 19.4% Bi, 56 nm thick sample show that these films are coherently strained to the GaAs substrates. This is in spite of the fact that the 14.2% and 19.4% GaAs_{1-x}Bi_x films have large (1.7% and 2.3%) lattice mismatches with the GaAs substrate. Figure 3 shows an example of one of the (224) RSM's for the 14.2% Bi sample, which is layer (b) in Fig. 2. The upper peak is from the GaAs substrate and the lower peak is from the GaAs_{1-x}Bi_x film. The in-plane component of the film peak (q_x) exactly matches the substrate to within the measurement error (dashed yellow line), indicating that the film is fully strained to the GaAs substrate. In fully relaxed films, the off axis planes have no tilt with respect to the corresponding substrate planes. As a result, a fully relaxed film peak would lie on a line directed from the substrate peak to the origin indicated by the solid yellow line. Pendellösung fringes are also seen between the film and substrate peaks.

To obtain a relationship between the GaAs_{1-x}Bi_x lattice parameter and the Bi content, RBS measurements were performed on selected pseudomorphic GaAs_{1-x}Bi_x/GaAs samples. Figure 4 presents RBS spectra together with SIMNRA simulations for several samples. The peak near 1.9 MeV in each spectrum corresponds to backscattering from Bi atoms

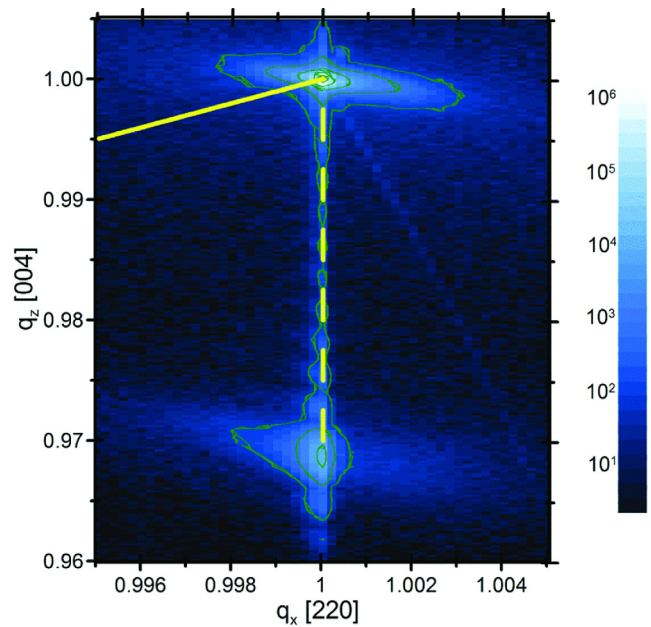


FIG. 3. (224) Reciprocal space map for a 53 nm thick 14.2% Bi film on a GaAs substrate (layer (b) in Fig. 2). The horizontal and vertical scales are the relative in-plane and out-of plane reciprocal space q vectors. The upper peak corresponds to the GaAs substrate and the lower peak is the GaAs_{1-x}Bi_x epilayer. The solid yellow line points to the origin, indicating the line where a 100% relaxed film would lie. The dashed yellow line shows the direction of a 100% strained film (no relaxation). The green contours are spaced by factors of 10 in intensity.

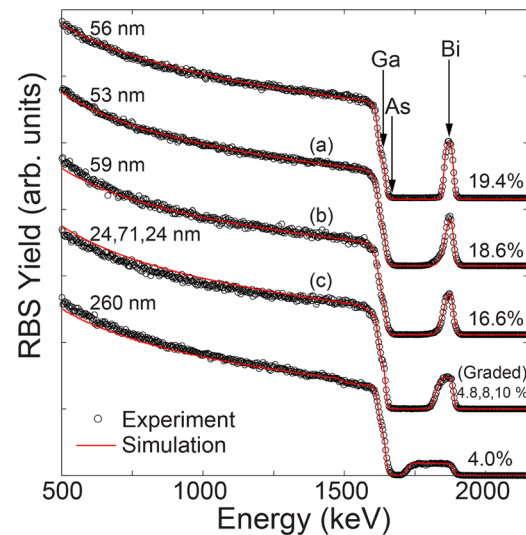


FIG. 4. RBS spectra (dots) and SIMNRA simulations (red lines) for several GaAs_{1-x}Bi_x films on GaAs. Spectra are offset vertically for clarity. The peak near 1.9 MeV for each spectrum corresponds to backscattering from Bi atoms in the GaAs_{1-x}Bi_x layer. The large step near 1.6 MeV corresponds to backscattering from Ga and As atoms in the layer and substrate. The labels ((a), (b), and (c)) correspond to the matching samples in Figs. 2, 4, and 5. For spectrum (c), a simulation with three layers gives a better fit than a single layer. The Bi composition and layer thickness of GaAs_{1-x}Bi_x films obtained from SIMNRA are shown in this figure. The Bi composition and layer thickness obtained from the dynamical simulations of the (004) HRXRD scans on the same samples are: (from bottom to top) (1) 3.7%, 255 nm (2) 9.7%, thickness not determined (3) 14.2%, 53 nm (4) 17.3%, 33 nm, and (5) 19.2%, ~40–60 nm.

in the $\text{GaAs}_{1-x}\text{Bi}_x$ layer. The large step near 1.6 MeV is due to backscattering from Ga and As atoms. The height of the Bi peak reflects the Bi content, while the width is proportional to the layer thickness. This information can be used to determine the uniformity of the Bi composition. For thin layers that do not result in flat-top peaks, the Bi content is determined by fitting the shape of the peak. In the thin sample limit, the RBS peak measures the product of the Bi content and the film thickness. The uncertainty in the Bi content of the thick 4% sample determined by RBS is $4.0 \pm 0.1\%$. The thinner, high Bi content layers have larger uncertainties: for example, $18.6 \pm 3\%$ and $16.6 \pm 2.5\%$ in the case of samples (a) and (b) in Fig. 4. For sample (c), a three layer simulation gives a better fit than a single layer, suggesting that the Bi content is not uniform over the layer thickness. This sample corresponds to the 9.7% film in Fig. 2, which has a broad (004) HRXRD scan with no pendellösung fringes.

The pseudomorphic and free standing lattice parameters for $\text{GaAs}_{1-x}\text{Bi}_x$ layers ($0 \leq x \leq 19.4\%$) on GaAs are shown as a function of Bi content in the inset of Fig. 2. The lattice parameters were measured from (004) HRXRD scans while the Bi contents were determined from RBS. With (004) strain information, the relaxed lattice parameter for these films is calculated assuming a constant Poisson ratio of 0.31 (black circles),¹⁵ which is the Poisson ratio for GaAs.^{16,17} This assumption is valid for dilute $\text{GaAs}_{1-x}\text{Bi}_x$ alloys, but might cause error for high Bi content films, as the effect of Bi alloying on the elastic constants of $\text{GaAs}_{1-x}\text{Bi}_x$ is unknown. Fitting a line to the relaxed data and assuming Vegard's law and that the layers are pseudomorphic, and then extrapolating to 100%, Bi yields a GaBi relaxed lattice constant of $6.33 \pm 0.05 \text{ \AA}$, in agreement with the earlier reported result of $6.33 \pm 0.06 \text{ \AA}$ obtained from similar experiments on $\text{GaAs}_{1-x}\text{Bi}_x/\text{GaAs}$ films with much lower Bi concentrations (up to 3.1% Bi¹⁸). This result is also in good agreement with the value of 6.328 \AA obtained from density functional theory calculations.¹⁹ The uncertainty in the lattice constant is the statistical error in the fit to the data and does not include systematic errors. The GaBi lattice constant of $6.33 \pm 0.05 \text{ \AA}$ determined here is larger than other reported values, also obtained by extrapolation of RBS and HRXRD data, namely: $6.272 \pm 0.005 \text{ \AA}$ from $\text{GaSb}_{1-x}\text{Bi}_x/\text{GaSb}$ films with up to 9.6% Bi,⁸ and 6.23 \AA from $\text{GaAs}_{1-x}\text{Bi}_x/\text{GaAs}$ films with up to 4.8% Bi.²⁰ The reason for the difference in the various experimental measurements is not known. A different choice of Poisson ratio makes a small difference. In Ref. 20, a Poisson ratio of 0.334 was used instead of 0.31. If we had used 0.334, the GaBi lattice constant would have been 6.30 \AA rather than 6.33 \AA . In Ref. 8, the host compound was GaSb not GaAs with a different set of elastic constants. The extrapolated GaBi lattice constant is used in the LEPTOS dynamical diffraction model to determine the Bi composition and layer thickness of each pseudomorphic film in Fig. 2 as noted above.

The $\text{GaAs}_{1-x}\text{Bi}_x$ lattice constant could, in principle, be subject to systematic errors associated with excess As incorporation. It is well-known that excess As incorporates in GaAs at low growth temperature and that this effect

increases the lattice constant.²¹ Under standard As-rich growth conditions at 220°C (the lowest $\text{GaAs}_{1-x}\text{Bi}_x$ growth temperatures used in our study), the compressive strain due to the excess As would be comparable to that for 0.3% Bi incorporation. However, excess As incorporation is substantially reduced for growth at or below stoichiometric As:Ga flux ratios,²¹ which is the case for the $\text{GaAs}_{1-x}\text{Bi}_x$ layers in this paper. Therefore, excess As incorporation is not expected to induce significant compressive strain in the $\text{GaAs}_{1-x}\text{Bi}_x$ films discussed here.

Figure 5 shows the normalized transmission spectra ($T_{\text{GaAsBi}}/T_{\text{GaAs}}$) of several $\text{GaAs}_{1-x}\text{Bi}_x$ films. For photon energies below the GaAs bandgap, 1.42 eV, the $\text{GaAs}_{1-x}\text{Bi}_x$ layer partially absorbs the incident light. The absorption edge is strongly red-shifted toward lower photon energies with increasing Bi content. At low photon energies below the $\text{GaAs}_{1-x}\text{Bi}_x$ absorption edge, the epilayers show maximum transmissivity near unity, indicating that there is weak sub-gap absorption and the refractive index of the layers is similar to that of the GaAs substrate. Although the refractive index of $\text{GaAs}_{1-x}\text{Bi}_x$ increases slightly with Bi content,²² the effect on the reflectivity is smaller than the measurement error. To confirm this observation, the change in reflectivity between a thin $\text{GaAs}_{1-x}\text{Bi}_x/\text{GaAs}$ heterostructure and a GaAs substrate is calculated from the optical constant data in Ref. 22. This calculation shows that the reflectivity of a thin 50 nm 7.5% Bi layer on GaAs deviates by $\sim 0.5\%$ from GaAs in the 0.2–0.8 eV range. Despite the excellent interface quality in most samples, no interference fringes are observed in the spectra, due to the small difference between the refractive indices of substrate and the epilayer. Therefore, multiple reflections within the $\text{GaAs}_{1-x}\text{Bi}_x$ layer are neglected and the absorption coefficient, α , can be well approximated by

$$\alpha(E) = -\frac{1}{d} \ln \left(\frac{T_{\text{GaAsBi}}}{T_{\text{GaAs}}} \right), \quad (1)$$

where d is the layer thickness and E is the photon energy. Below the bandgaps, the transmission spectra show small offsets ($\sim \pm 0.7\%$) from unity, likely due to differences in

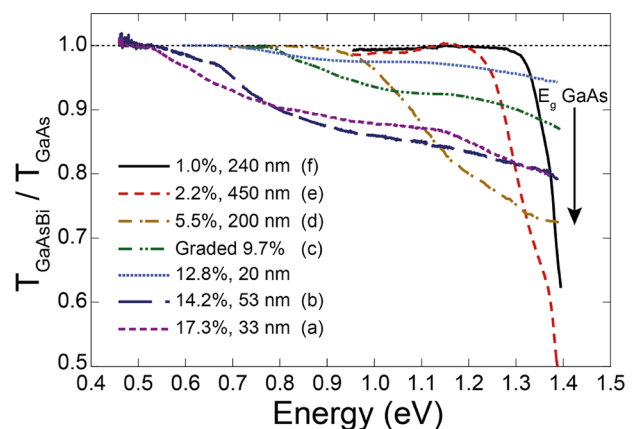


FIG. 5. Room temperature optical transmission spectra of several $\text{GaAs}_{1-x}\text{Bi}_x/\text{GaAs}$ heterostructures divided by the GaAs substrate transmission spectrum ($T_{\text{GaAsBi}}/T_{\text{GaAs}}$). The labels are the same as for the samples in Figs. 2 and 4.

surface scattering caused by differences in sample roughness. The offsets measured below the bandgap are subtracted from each transmission spectrum in Fig. 5, and the resulting spectra are used to derive α from Eq. (1), as shown in Fig. 6(a). The experimental data are not accurate enough to determine the absorption below about 100 cm^{-1} . Figure 6(a) also shows the absorption coefficient of a $350\text{ }\mu\text{m}$ thick semi-insulating GaAs reference substrate. For this sample, absorption values above $\sim 200\text{ cm}^{-1}$ are omitted as they have low signal levels. The GaAs absorption coefficient is also calculated from literature values of the extinction coefficient,²³ $\alpha = 4\pi\kappa/\lambda$, and is shown for comparison.

For a direct bandgap semiconductor, parabolic band theory predicts an abrupt absorption edge with the form $\alpha(E) = A\sqrt{E - E_g}$ above the band tail,²⁴ where A is a constant. Therefore, a plot of α^2 vs. photon energy should demonstrate a linear relation and provide an estimate of E_g from the x-intercept. The square of the absorption coefficient is plotted for selected GaAs_{1-x}Bi_x layers in Fig. 6(b). For most of the samples, α^2 is approximately linear with photon energy with similar slopes up to $\alpha^2 \sim 10^8\text{ cm}^{-2}$. This supports the notion that GaAs_{1-x}Bi_x has a direct optical bandgap up to at least 18% Bi. Band tails are visible at low absorption, resulting in a deviation from the linear behavior. The bandgaps are obtained by least square fitting the straight lines to the absorption curves from $\alpha^2 = 2 \times 10^7\text{ cm}^{-2}$ (below this the

band tails dominate) to $\alpha^2 = 1.0\text{--}1.7 \times 10^8\text{ cm}^{-2}$, and then extrapolating these linear fits to zero (solid lines). The samples with high Bi contents of 17.3% and 14.2% show bandgaps of 0.55 ± 0.04 and 0.66 ± 0.02 eV, respectively.

The sample with 9.7% Bi shows more than one absorption slope due to composition variations in the growth direction. These variations also show up in the RBS and HRXRD results (layer c in Figs. 2 and 4). Both RBS and HRXRD indicate that this film has Bi content above 8%. The RBS data can be fitted with three sub-layers: (1) 4.8% Bi, 24 nm (2) 8% Bi, 71 nm, and (3) 10% Bi, 24 nm. If the total thickness of the 8% and 10% Bi layers (95 nm) is used in the calculation of the absorption coefficient, we obtain curve I in Fig. 6(b). The slope of the absorption spectrum is anomalously low in this case. The low energy absorption is controlled by the high Bi content portion of the film, which is thinner than the assumed value. If we repeat the calculation of the absorption spectrum using the RBS value for the thickness of the high Bi content component only (24 nm), we obtain curve II in Fig. 6(b). The slope of this curve is better aligned with the other samples.

In the region below the bandgap, the absorption coefficient decreases exponentially with the decrease in photon energy as shown in Fig. 6(a). The width of the exponential tail or Urbach energy is often taken as a measure of the structural quality of crystalline and amorphous semiconductors.^{25,26} The optical absorption in the Urbach region can be described by

$$\alpha(E, T) = \alpha_g \exp\left(\frac{E - E_g}{E_0(T)}\right), \quad (2)$$

where E_g is the bandgap energy, α_g is the value of the absorption coefficient at the bandgap, and E_0 is the characteristic energy of the exponential absorption edge (Urbach energy). The parameter $E_0(T)$ is composed of a thermal phonon interaction component and a temperature independent structural disorder component.²⁵⁻²⁷

As shown by the solid lines in Fig. 6(a), the Urbach energy of the GaAs_{1-x}Bi_x layers is determined from exponential fits below the bandgaps. The inset shows the measured values of E_0 as a function of Bi content. E_0 increases linearly from 24 to 40 meV as Bi content increases from 1% to 5.5%. However, the higher Bi content samples ($x > 9\%$) show a constant E_0 of 25 meV. Similar anomalous changes in the nature of the shallow electronic defects have been observed in other measurements for Bi concentrations near 5%, which we summarize here. In magnetic field dependent photoluminescence experiments, Pettinari *et al.*²⁸ found that the exciton reduced mass increased with Bi concentration up to about 3% then decreased above 6%. Far-infrared photoinduced absorption measurements as a function of magnetic field, also by Pettinari, showed that above 5.6% Bi, Bi-related acceptor states are no longer present.²⁹ The intensity and linewidth of photoluminescence in GaAs_{1-x}Bi_x were observed to peak at $\sim 5\%$ Bi.^{1,28} A defect contribution was observed in the linewidth of PL from GaAs_{1-x}Bi_x/GaAs quantum wells for $x = 3.5\%$, but there was no defect contribution to the linewidth for $x = 6\%$.³⁰ Bi short range ordering

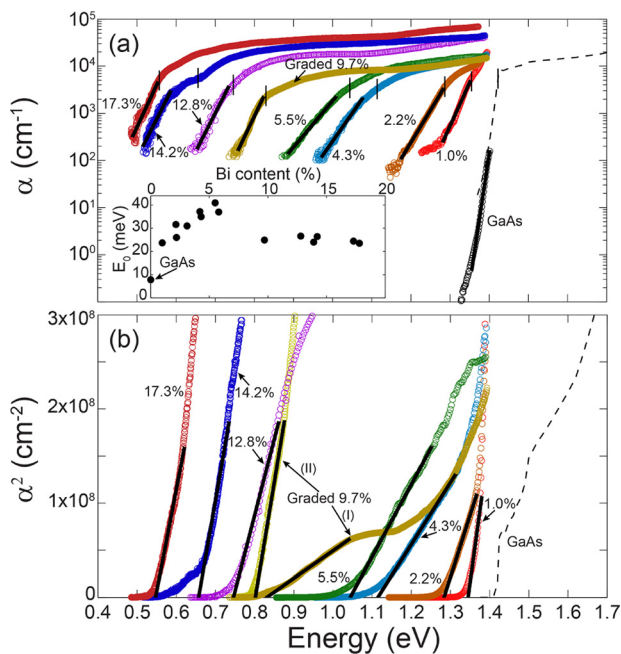


FIG. 6. (a) Absorption coefficient α and (b) α^2 vs. photon energy for several GaAs_{1-x}Bi_x films and for a $350\text{ }\mu\text{m}$ thick semi-insulating GaAs substrate. The dashed line is calculated from GaAs extinction coefficient data in Ref. 23. E_g of each layer is estimated from linear fits to α^2 from $\alpha^2 = 2 \times 10^7\text{ cm}^{-2}$ to $\alpha^2 = 1.0\text{--}1.7 \times 10^8\text{ cm}^{-2}$ extrapolated to zero absorption (solid lines in (b)). The location of the bandgap in each layer is shown with vertical solid dashes in Figure (a). The absorption coefficient of the graded 9.7% layer is calculated by considering two thicknesses: (I) RBS total thickness of 8% and 10% Bi-containing layers (95 nm) and (II) RBS thickness of the 10% layer only (24 nm). The Urbach parameters, E_0 , are determined from exponential fits below the bandgaps (solid lines in a). The inset summarizes the measured values of E_0 as a function of the Bi content at room temperature.

was observed for $x = 2.4\%$, but this ordering vanished for $x > 5.4\%$ Bi.³¹ These properties reveal a complex evolution of the band edge states in dilute GaAs_{1-x}Bi_x alloys with increasing Bi concentration. The increase in E_0 at low Bi concentrations may be due to the formation of localized states above the valence band associated with Bi dimers or larger clusters.^{1,28,32} The subsequent decrease in E_0 at high Bi concentrations could then be considered as a transition from an alloy dominated by disorder associated with Bi to a more conventional III-V semiconductor alloy, once the Bi-associated localized states merge into a band²⁸ or get overtaken by extended band states at higher Bi concentrations.

The resulting E_0 values are 3–6 times larger than the Urbach energy for bulk GaAs, $E_0 = 7.7$ meV, indicating that the addition of Bi to GaAs, broadens the band edge. The results obtained here are consistent with other published data, for example, the 7.5 meV reported earlier for GaAs,²⁷ the 21–24 meV observed in GaAs_{0.94}Bi_{0.06}/GaAs diodes³³ and ~ 30 meV reported for a GaAs_{0.95}Bi_{0.05} quantum well structure.³²

Figure 7 shows room temperature PL spectra for the GaAs_{1-x}Bi_x/GaAs layers with up to 10.5% Bi content. The highest energy peak in each spectrum corresponds to the band edge emission which shifts to lower energy with an increasing Bi content, as expected. In thick layers ($d > 200$ nm), a lower energy emission peak between 1.10 eV to 1.21 eV is also observed. This peak is believed to correspond to emission from defect states in the bandgap. It should be noted that the low energy emission is not generally observed in thin samples ($\sim d < 50$ nm) grown under the same conditions. In thin samples, the electron-hole pairs have a reduced diffusion length, making it more difficult for carriers to find the isolated deep levels associated with defect states.

The PL peak intensity of thin GaAs_{1-x}Bi_x layers are also shown in Fig. 7, relative to the intensity of a bulk semi-insulating GaAs reference substrate. Strong luminescence is observed from thin GaAs_{1-x}Bi_x layers with up to 5.7% Bi content. The 10.5% Bi layer shows weak PL emission; however, this sample is thinner than the other layers and was grown at a lower substrate temperature (260 °C). Other

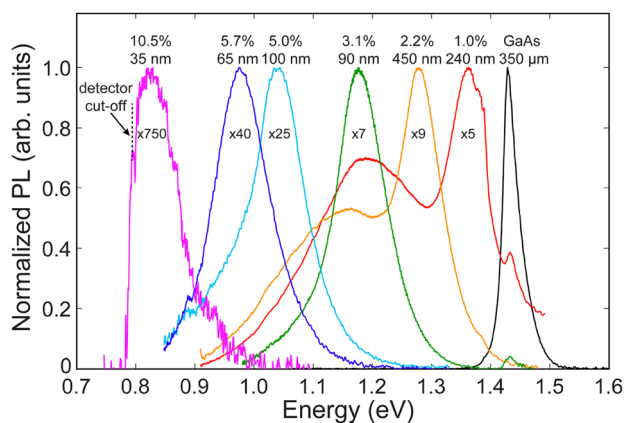


FIG. 7. Room temperature photoluminescence spectra of GaAs_{1-x}Bi_x/GaAs layers and a semi-insulating GaAs substrate. The scale factors indicate the peak intensity of the GaAs_{1-x}Bi_x thin films relative to the GaAs substrate.

layers in this figure were grown at higher temperatures (300–350 °C). In general, GaAs_{1-x}Bi_x layers show broader PL emission than bulk GaAs (~ 0.1 eV vs. 0.03 eV FWHM). This is likely due to the distribution of localized levels close to the band edge associated with Bi clusters.³⁴

The room temperature bandgaps of GaAs_{1-x}Bi_x alloys ($0 \leq x \leq 17.8\%$) obtained from absorption edge measurements as well as from the PL peak position ($0 \leq x \leq 10.5\%$) are shown in Fig. 8. PL data from Lu *et al.*¹ and density functional theory (DFT)¹⁹ calculations are also presented for comparison. The DFT curve is shifted downward to match the room temperature GaAs bandgap energy of 1.42 eV. The experimental results in this figure are for pseudomorphic films under in-plane compressive stress, while the DFT calculations are for unstrained material. The E_g acquired from PL experiments is at a lower energy than the E_g acquired from the optical absorption experiments due to the PL emission taking place below the bandgap in the tail states.

The composition dependence of E_g in III-V semiconductor alloys is commonly described by interpolation between the binary end compounds using a quadratic equation. For the ternary GaAs_{1-x}Bi_x, the interpolation formula is as follows:

$$E_{\text{GaAs}_{1-x}\text{Bi}_x} = xE_{\text{GaBi}} + (1-x)E_{\text{GaAs}} - bx(1-x), \quad (3)$$

where b is the bowing parameter and E_{GaBi} and E_{GaAs} are the bandgap energies of GaBi and GaAs, respectively. As E_{GaBi} is unknown, there are two parameters, E_{GaBi} and b , in the above equation. For most III-V alloys, a constant bowing parameter is sufficient to fit experimental data. However, in the case of highly mismatched alloys, such as GaAsN, GaAsBi, and InAlN, a composition-dependent bowing

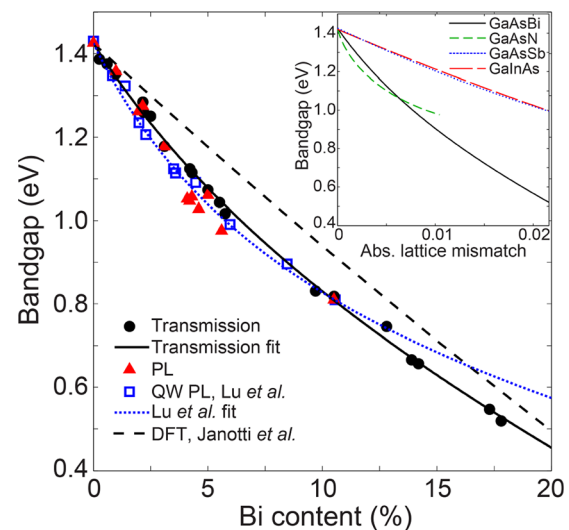


FIG. 8. Compositional dependence of the GaAs_{1-x}Bi_x bandgap, from optical absorption and PL measurements. The solid line is a fit to the absorption data using a Bi concentration dependent bowing coefficient as discussed in the text. PL data and a fit function from Lu *et al.*¹ along with a DFT calculation,¹⁹ shifted to match the room temperature E_g of GaAs, are shown for comparison. The inset shows E_g as a function of lattice mismatch for bandgap lowering ternary alloys with In,³ Sb,⁴ N⁵, and Bi (this work) on GaAs substrates. The range of fits for GaAsBi and GaAsN are shown for experimentally measured compositions (i.e., max 18% Bi and 5% N content).

parameter has been used.^{1,5,35} In the case of GaAs_{1-x}Bi_x alloy, Lu *et al.*¹ showed that PL data can fit well with a bowing parameter that decreases monotonically with increasing Bi content, of the form:

$$b(x) = \frac{\alpha}{1 + \beta x}. \quad (4)$$

The relation is analogous to that used earlier for InAlN alloys.³⁵ This relation is found to provide a good fit to our experimental absorption data. From the expression for the composition dependent bowing parameter in Eq. (4), a best fit to the absorption data is obtained with $E_{GaBi} = -1.60$ eV, $\alpha = 5.63$ and $\beta = 7.34$. This fit is shown as the solid line in Fig. 8. An earlier fit to lower Bi concentration samples by Lu *et al.*¹ using the same equation found the following different fitting parameters: $E_{GaBi} = -0.36$ eV, $\alpha = 9.5$ and $\beta = 10.4$. The fit from Lu *et al.* is plotted in Fig. 8 as a dotted line. This curve does not fit the bandgap of the high Bi concentration samples with $x > 10\%$ in Fig. 8. As a result, the Lu *et al.* fit predicts a zero bandgap at [Bi] = 64%, whereas the new fit to samples with Bi concentrations up to 17.8% predicts a zero bandgap at [Bi] = 35%. Since the new fit in this paper is based on data for samples with higher Bi concentration, the extrapolation to zero bandgap is shorter, and the zero bandgap point is therefore expected to be more reliable; nevertheless, being an extrapolation, it is difficult to determine the accuracy of the inferred zero bandgap point. In the low Bi concentration range ($x < 12\%$), our results are in close agreement with bandgap estimates from valence band anti-crossing calculations.^{36–38}

The inset in Fig. 8 compares the dependence of the bandgap on lattice mismatch for bandgap lowering ternary alloys with In,³ Sb,⁴ N,⁵ and Bi (this work) on GaAs substrates. The GaAsBi curve is taken from the fit to the optical absorption bandgap in the main figure. The range of fits for GaAsBi and GaAsN are shown for experimentally tested concentrations (i.e., max 18% Bi and 5% N content). Below ~ 1.06 eV ($x \geq 5.5\%$ Bi), GaAsBi has the least lattice mismatch from GaAs of any alloy, including GaAsN, for a given bandgap. This unmatched bandgap reduction makes GaAsBi appealing for extending the wavelength of optoelectronics devices on GaAs substrates as well as substrates with larger lattice parameter like InP, beyond what traditional alloying elements offer.

CONCLUSIONS

The composition dependence of the bandgap of pseudomorphic GaAs_{1-x}Bi_x layers ($0 \leq x \leq 17.8\%$) on GaAs substrates has been measured with optical transmission and PL spectroscopies. All samples show direct bandgaps. The bandgap energy decreases with increasing Bi content, reaching $E_g = 0.52$ eV at 17.8% Bi. The absorption coefficient below the bandgap reveals exponential band tails with 3–6 times larger Urbach energy than that of bulk GaAs. The Urbach parameter is found to increase from 24 to 40 meV with increasing Bi in the $1\% < x < 5.5\%$ range; at higher concentrations $x > 9\%$, it remains constant at about 25 meV. This dependence on Bi content is consistent with literature

reports of changes in the nature of the shallow electronic defects near $x \sim 5\%$. The relationship between lattice constant and Bi content has been measured by RBS and HRXRD up to 19.4% Bi. Below $E_g \sim 1.06$ eV, GaAs_{1-x}Bi_x has less mismatch to GaAs than any other ternary GaAs alloy, including GaAsN, for a given bandgap. The strong bandgap reduction per unit strain in GaAs_{1-x}Bi_x alloys shows promise for extending the wavelength range of devices on GaAs, beyond what other III–V alloys offer. Extrapolating our results, GaAs_{1-x}Bi_x lattice matched to InP is expected to have a bandgap of ~ 0.1 eV or $\sim 10 \mu\text{m}$.

ACKNOWLEDGMENTS

We thank NSERC for financial support. The authors thank Lucas Chrostowski for generously allowing us to use his equipment.

- ¹X. Lu, D. A. Beaton, R. B. Lewis, T. Tiedje, and Y. Zhang, *Appl. Phys. Lett.* **95**, 041903 (2009).
- ²S. Francoeur, M.-J. Seong, A. Mascarenhas, S. Tixier, M. Adamcyk, and T. Tiedje, *Appl. Phys. Lett.* **82**, 3874 (2003).
- ³R. Moon, G. Antypas, and L. James, *J. Electron Mater.* **3**(3), 635–644 (1974).
- ⁴G. Liu, S. Chuang, and S. Park, *J. Appl. Phys.* **88**, 5554 (2000).
- ⁵U. Tisch, E. Finkman, and J. Salzman, *Appl. Phys. Lett.* **81**, 463 (2002).
- ⁶C. A. Broderick, M. Usman, S. J. Sweeney, and E. P. O'Reilly, *Semicond. Sci. Technol.* **27**, 094011 (2012).
- ⁷R. B. Lewis, M. Masnadi-Shirazi, and T. Tiedje, *Appl. Phys. Lett.* **101**, 082112 (2012).
- ⁸M. K. Rajpalke, W. M. Linhart, M. Birkett, K. M. Yu, J. Alaria, J. Kopaczek, R. Kudrawiec, T. S. Jones, M. J. Ashwin, and T. D. Veal, *J. Appl. Phys.* **116**, 043511 (2014).
- ⁹I. C. Sandall, F. Bastiman, B. White, R. Richards, D. Mendes, J. P. R. David, and C. H. Tan, *Appl. Phys. Lett.* **104**, 171109 (2014).
- ¹⁰I. P. Marko, Z. Batool, K. Hild, S. R. Jin, N. Hossain, T. J. C. Hosea, J. P. Petropoulos, Y. Zhong, P. B. Dongmo, J. M. O. Zide, and S. J. Sweeney, *Appl. Phys. Lett.* **101**, 221108 (2012).
- ¹¹Y. Zhong, P. B. Dongmo, J. P. Petropoulos, and J. M. O. Zide, *Appl. Phys. Lett.* **100**, 112110 (2012).
- ¹²R. B. Lewis, J. A. Mackenzie, T. Tiedje, D. A. Beaton, M. Masnadi-Shirazi, V. Bahrami-Yekta, K. P. Watkins, and P. M. Mooney, *J. Vac. Sci. Technol. B* **31**, 03C116 (2013).
- ¹³R. B. Lewis, V. Bahrami-Yekta, M. J. Patel, T. Tiedje, and M. Masnadi-Shirazi, *J. Vac. Sci. Technol. B* **32**, 02C102 (2014).
- ¹⁴M. Mayer, *AIP Conf. Proc.* **475**, 541 (1999).
- ¹⁵D. K. Bowen and B. K. Tanner, *High Resolution X-ray Diffractometry and Topography* (CRC Press, 2005).
- ¹⁶W. A. Brantley, *J. Appl. Phys.* **44**, 534 (1973).
- ¹⁷M. Krieger, H. Sigg, N. Herres, K. Bachem, and K. Köhler, *Appl. Phys. Lett.* **66**, 682 (1995).
- ¹⁸S. Tixier, M. Adamcyk, T. Tiedje, S. Francoeur, A. Mascarenhas, P. Wei, and F. Schiettekatte, *Appl. Phys. Lett.* **82**, 2245 (2003).
- ¹⁹A. Janotti, S.-H. Wei, and S. B. Zhang, *Phys. Rev. B* **65**, 115203 (2002).
- ²⁰Y. Takehara, M. Yoshimoto, W. Huang, J. Saraie, K. Oe, A. Chayahara, and Y. Horino, *Jpn. J. Appl. Phys.* **45**, 67 (2006).
- ²¹M. Missous, *Microelectron. J.* **27**, 393 (1996).
- ²²S. Tuménas, V. Karpus, K. Bertulis, and H. Arwin, *Phys. Status Solidi C* **9**, 1633 (2012).
- ²³*Handbook of Optical Constants of Solids*, edited by E. D. Palik (Academic Press, 1998).
- ²⁴J. I. Pankove, *Optical Processes in Semiconductors* (Prentice-Hall, New Jersey, 1971).
- ²⁵F. Urbach, *Phys. Rev.* **92**, 1324 (1953).
- ²⁶G. D. Cody, T. Tiedje, B. Abeles, B. Brooks, and Y. Goldstein, *Phys. Rev. Lett.* **47**, 1480 (1981).
- ²⁷S. R. Johnson and T. Tiedje, *J. Appl. Phys.* **78**(9), 5609 (1995).
- ²⁸G. Pettinari, A. Polimeni, J. H. Blokland, R. Trotta, P. C. M. Christianen, M. Capizzi, J. C. Maan, X. Lu, E. C. Young, and T. Tiedje, *Phys. Rev. B* **81**, 235211 (2010).

- ²⁹G. Pettinari, H. Engelkamp, P. C. M. Christianen, J. C. Maan, A. Polimeni, M. Capizzi, X. Lu, and T. Tiedje, *Phys. Rev. B* **83**, 201201(R) (2011).
- ³⁰Y. I. Mazur, V. G. Dorogan, M. Benamara, M. E. Ware, M. Schmidbauer, G. G. Tarasov, S. R. Johnson, X. Lu, S-Q. Yu, T. Tiedje, and G. J. Salamo, *J. Phys. D: Appl. Phys.* **46**, 065306 (2013).
- ³¹G. Ciatto, M. Thomasset, F. Glas, X. Lu, and T. Tiedje, *Phys. Rev. B* **82**, 201304(R) (2010).
- ³²C. Gogineni, N. A. Riordan, S. R. Johnson, X. Lu, and T. Tiedje, *Appl. Phys. Lett.* **103**, 041110 (2013).
- ³³C. J. Hunter, F. Bastiman, A. R. Mohmad, R. Richards, J. S. Ng, S. J. Sweeney, and J. P. R. David, *IEEE Photonics Technol. Lett.* **24**, 2191 (2012).
- ³⁴S. Imhof, A. Thranhardt, A. Chernikov, M. Koch, N. S. Koster, K. Kolata, S. Chatterjee, S. W. Koch, X. Lu, S. R. Johnson, D. A. Beaton, T. Tiedje, and O. Rubel, *Appl. Phys. Lett.* **96**, 131115 (2010).
- ³⁵E. Iliopoulos, A. Adikimenakis, C. Giesen, M. Heuken, and A. Georgakilas, *Appl. Phys. Lett.* **92**, 191907 (2008).
- ³⁶K. Alberi, J. Wu, W. Walukiewicz, K. M. Yu, O. D. Dubon, S. P. Watkins, C. X. Wang, X. Liu, Y.-J. Cho, and J. Furdyna, *Phys. Rev. B* **75**, 045203 (2007).
- ³⁷A. R. Mohmad, F. Bastiman, C. J. Hunter, R. D. Richards, S. J. Sweeney, J. S. Ng, J. P. R. David, and B. Y. Majlis, *Phys. Status Solidi B* **251**(6), 1276 (2014).
- ³⁸M. Usman, C. A. Broderick, A. Lindsay, and E. P. O'Reilly, *Phys. Rev. B* **84**, 245202 (2011).